Ultrasound in Med. & Biol., Vol. 42, No. 10, pp. 2478–2492, 2016

0301-5629/$ - see front matter

http://dx.doi.org/10.1016/j.ultrasmedbio.2016.06.001

● *Original Contribution*

THE APPLICATION OF CLINICAL LITHOTRIPTER SHOCK WAVES TO RNA NUCLEOTIDE DELIVERY TO CELLS

Sandra Nwokeoha, Robert Carlisle, and Robin O. Cleveland

Institute of Biomedical Engineering, Department of Engineering Science, University of Oxford, Oxford, United Kingdom

(*Received* 5 *January* 2016; *revised* 15 *April* 2016; *in final form* 2 *June* 2016)

Abstract—The delivery of genes into cells through the transfer of ribonucleic acids (RNAs) has been found to cause a change in the level of target protein expression. RNA-based transfection is conceptually more efficient than commonly delivered plasmid DNA because it does not require division or damage of the nuclear envelope, thereby increasing the chances of the cell remaining viable. Shock waves (SWs) have been found to induce cellular uptake by transiently altering the permeability of the plasma membrane, thereby overcoming a critical step in gene therapy. However, accompanying SW bio-effects include dose-dependent irreversible cell injury and cytotoxicity. Here, the effect of SWs generated by a clinical lithotripter on the viability and permeabilisation of three different cell lines *in vitro* was investigated. Comparison of RNA stability before and after SW exposure revealed no statistically significant difference. Optimal SW exposure parameters were identified to minimise cell death and maximise permeabilisation, and applied to enhanced green fluorescent protein (eGFP) messenger RNA (mRNA) or anti-eGFP small interfering RNA delivery. As a result, eGFP mRNA expression levels increased up to 52-fold in CT26 cells, whereas a 2-fold decrease in GFP expression was achieved after anti-eGFP small interfering RNA delivery to MCF-7/GFP cells. These results indicate that SW parameters can be employed to achieve effective nucleotide delivery, laying the foundation for non-invasive and high-tolerability RNA-based gene therapy. (E-mail: sandra.nwokeoha@eng.ox.ac.uk) **© 2016 The Authors. Published by Elsevier Inc. on behalf of World Federation for Ultrasound in Medicine & Biology. This is an open access article under the CC BY license (http://creativecommons.org/licenses/by/4.0/).**

Key Words: **Shock waves, High-amplitude acoustic waves, Ultrasound, Messenger RNA, Small interfering RNA, Gene therapy, Drug delivery.**

INTRODUCTION

Nucleic acid–based therapies provide a powerful approach to the treatment of genetic diseases, by introducing into target cells, healthy replacements of mutated or absent genes, or gene-specific inhibitory molecules; ultimately to reinstate typical cellular function either through the expression of normal protein or the repression of defective protein. However, biological and chemical vectors for delivery are limited by potential viral toxicity and poor targeting, respectively (Mehier-Humbert and Guy 2005). On the other hand, physical transfection systems for the delivery of nucleic acids have attracted substantial attention in recent years, as they permit accessibility to the target site and entry into the cell's cytosol. Such methods include electroporation, the gene gun, laser irradiation, magnetofection and microinjection. Notably, electroporation has achieved comparably high transfection levels, whereby up to 1000-fold increases in gene expression have been reported relative to the admittedly highly inefficient level achieved with standard plasmid DNA injection (Wells 2004). However, one common drawback all such methods share is the inability to access deep-seated tissues without compromising safety. As a result, sonoporation, the process of transiently permeabilising the cell membrane using ultrasound, provides the most practical and least invasive device-based option when deep access is needed (Mo et al. 2012). Nonetheless, the efficacy of sonoporation strongly depends on the acoustic parameters of the employed technology, because a trade-off exists between maintaining high cell viability and achieving nucleotide uptake.

Address correspondence to: Sandra Nwokeoha, Institute of Biomedical Engineering, Old Road Campus Research Building, University of Oxford, OX3 7DQ, Oxford, UK. E-mail: sandra.nwokeoha@eng.ox.ac.uk

Lithotripsy technology has been used clinically for more than 30 years to fragment kidney stones extracorporeally (Chaussy et al. 1980; Cleveland and McAteer 2007), with later applications in macromolecule (Delius and Adams 1999; Gambihler et al. 1994) and plasmid DNA transfer into tumours (Bao et al. 1998; Miller et al. 1999; Song et al. 2002) and chondrocytes *in vitro* (Murata et al. 2007). Lithotripter-generated shock waves are characterized as high-amplitude short-pulse acoustic waves that exert mechanical forces on the focal zone, through two known mechanisms: direct shear stress and the formation, growth and subsequent violent collapse of cavitation bubbles (Cleveland and McAteer 2007; Madersbacher and Marberger 2003). Transfer has been attributed to a transient disruption of the plasma membrane taking the shape of defects or pores at least 50 nm in diameter (Ben-Dor et al. 2000). The short duration of the shock wave pulse results in a temperature rise $<1°C$, producing negligible thermal effects (Huber et al. 1999). This aspect favours shock wave-assisted gene therapy over high-intensity focused ultrasound, as the latter results in tissue heating that may damage the cells, thereby compromising viability, which is a prerequisite for gene expression, as well as potentially affecting the functionality of the delivered nucleotide.

A wide range of shock wave-induced DNA transfection efficiencies has been reported *in vitro*. Lauer et al. (1997) observed poor permeabilisation levels of between 0.1% and 0.5%, which were found to be independent of the cell concentration utilised. Huber et al. (1999) optimised their shock wave exposure of cells and determined a threefold stimulation enhancement of reporter gene expression. The introduction of cavitation nuclei was deemed necessary for robust shock wave effects by Miller et al. (1999) and was achieved by intentionally having residual air in their cell samples. More recently, Millán-Chiu et al. (2014) reported that a maximum of 2.9% of cells exposed to shock waves were transfected based on refined but suboptimal parameter settings. In contrast, Bao et al. (1998) found that at 50% cell viability, cells exposed to 200 shock waves had a 50-fold increase in reporter gene expression per million cells.

The introduction of nucleotide into the cell as DNA has seen faster research uptake compared with RNA because of its inherent stability. In contrast, RNA is labile and more difficult to synthesise. Nonetheless, mRNA provides greater reliability of transfection because it does not require nuclear entry for protein expression and, thus, is not limited to cycling cells (Bettinger et al. 2001; Gilboa and Vieweg 2004). As such, host genome integration and risk of insertion-based mutagenesis are averted (Pinel et al. 2014). Moreover, mRNA promotes relatively faster reporter gene production, as the initial transcription phase in gene expression is foregone (Ponsaerts et al. 2003). Furthermore, unlike DNA, mRNA is free from immunogenic CpG motifs that may elicit host immune response (Pinel et al. 2014).

For the reduced translation of aberrant cellular protein, small interfering RNA (siRNA), which also has a cytoplasmic site of action, has been reported to achieve effective gene knockdown (Bertrand et al. 2002) through the command of sequence-complementary mRNA degradation (Hall 2004). As such, siRNA holds promise in the treatment of oncogenes and other disorder-generating gene products. Hence, RNA may be particularly suited to delivery by lithotripsy because, provided the right parameters can be identified, opening of the plasma membrane may be achieved without needing to impart damage to the nucleus.

To date, shock waves have not yet been exploited for mRNA-based transgene expression, and in the context of *in vitro* studies, the application of tissue-mimicking materials (TMMs) has been scarce. Similarly, there are few reports of shock wave-induced siRNA delivery in the literature. In addition, studies detailing shock wave dose-dependent bio-effects were performed using early-generation technologies (reviewed in Brümmer et al. 1990), with a considerable number of studies using such machines as the Dornier XL1 lithotripter (Brümmer et al. 1989; Delius and Adams 1999; Gambihler et al. 1994; Lauer et al. 1997) and the Siemens Lithostar (Huber et al. 1999; Oosterhof et al. 1989), which are no longer available. In view of newer clinical lithotripter technology, which provides an enabling pathway to translation, little, if any, work has been conducted on shock wave-mediated cancer treatment at the cellular level.

Here, we present studies aimed at achieving and describing delivery of RNA to cells using a state-of-the-art clinical shock wave source. We report cell line-based optimal shock wave parameters for the enhancement of RNA transfection of cancer cells.

METHODS

Cell lines and cell culture

Mouse colorectal carcinoma CT26.WT cells (ATCC, CRL-2638; American Type Culture Collection, Rockville, MD, USA), kindly provided by the Department of Oncology (Oxford University, Oxford, UK), were grown in Roswell Park Memorial Institute (RPMI)-1640 medium (Sigma-Aldrich, St. Louis, MO, USA) supplemented with 10% fetal bovine serum (FBS, Thermo Fisher Scientific, Waltham, MA, USA), in a humidified atmosphere containing 5% CO_2, at 37°C. Cells were grown to a minimum of 90% confluence and $\geq$95% cell viability for use in shock wave experiments. Cells were washed with Dulbecco's

phosphate-buffered saline solution (Thermo Fisher Scientific), harvested by brief trypsinisation and neutralised with medium twice the volume of the trypsin–EDTA (Thermo Fisher Scientific). A cell pellet was formed by centrifugation at 300*g* for 5 min and re-suspended in serum-containing medium. To ensure cell density and homogeneity, the prepared cell suspension was agitated using a vortex mixer for a few seconds before counting. Total cell counting was performed using the trypan blue (Thermo Fisher Scientific) dye exclusion method and a haemocytometer. A cell stock solution was then prepared by extracting the total number of cells required from the cell suspension and diluting with medium to the total required volume. The stock solution was spun once more before dispensing into sample units.

Two other cell lines were similarly cultured: immortalised human kidney (HK-2) cells (ATCC, CRL-2190) and human breast cancer (MCF-7) cells stably expressing green fluorescent protein (GFP, AKR-211, Cell Biolabs, San Diego, CA, USA). These were treated using 10% fetal bovine serum–supplemented Dulbecco's modified Eagle medium (Thermo Fisher Scientific) in lieu of RPMI-1640.

Shock wave generation and setup

Shock waves were generated with the Storz Modulith SLX-F2 lithotripter (Storz Medical, Kreuzlingen, Switzerland) with the kind permission of Oxford Stone Group (Churchill Hospital, Oxford, UK). The lithotripter consisted of an electromagnetic cylinder coil with dual focal zones. The wide focus zone was applied to all experiments, with a nominal size of 9 × 50 mm (diameter × length) at peak positive pressures ranging from 5 to 90 MPa. Experiments were carried out in a water-filled tank with a low-density polyethylene membrane for shock waves to enter, which was coupled to the shock wave transducer by a thin layer of silicone oil. Cell samples were suspended underwater (Fig. 1a) and positioned centrally in the focus through fluoroscopic projections at 0° and 30° relative to the vertical axis.

Ideal experimental conditions for cells were created by heating the tank water to 37°C using a Grant GD100 water heater (Grant Instruments, Royston, UK). For experimental reproducibility, as well as in view of a lack of cavitation nuclei in non-gas-bearing body tissues, the water was degassed using a pinhole degasser for a minimum of 1 h.

Shock wave field characterisation

To determine the pressure at the focal point, the acoustic field was measured using a Müller-Platte polyvinylidene fluoride needle hydrophone (Article No. 100-100-1, Müller Instruments, Oberursel, Germany) with a 40-ns rise time. The signals produced by the hydrophone were recorded using a digital oscilloscope (Le Croy waveRunner 44 Xi, 400-MHz sampling rate, LeCroy, Santa Clara, CA, USA). The hydrophone was positioned using a manual three-axis linear stage. Measurements were taken along the lateral axes (x and y) in the focal region area, in increments of 1 mm for up to 10 mm, and along the propagation axis (z) in increments of 2–5 mm for up to 45 mm. Five waveforms were recorded at each location and converted to pressure using the calibration furnished by the manufacturer. The procedure was repeated with the hydrophone inside a vial only at the focal point.

Sample preparation and treatments

Polypropylene vials (T7813, Sigma-Aldrich) with a volume of 2 mL were filled with the suspended cells at a

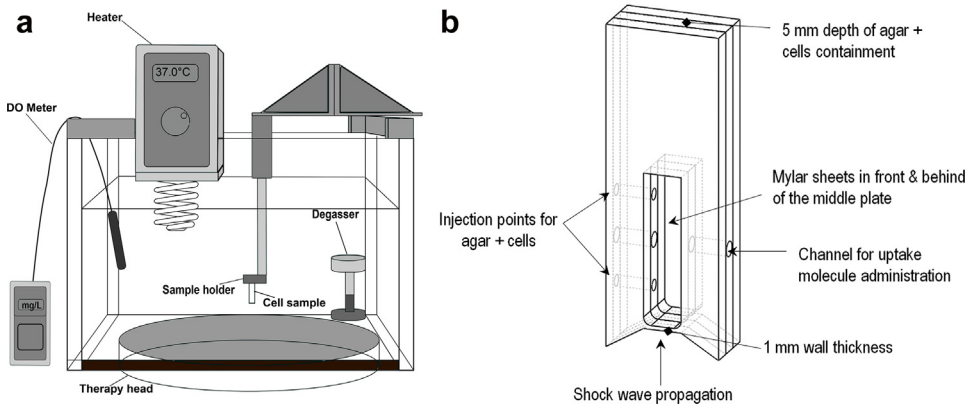

Fig. 1. (a) Shock wave permeabilisation equipment and setup. Shock waves were generated through a 43-L water tank, fitted above the shock wave source. Cell samples were supported by a sample holder, and maintained at 37°C with a thermostatic heater. The flow degasser reduced oxygen content to 1–3 mg/L. (b) Custom-made tissue phantom vessel for RNA transfection. The dimensions of the agar + cells containment were 10 × 5 × 40 mm (L × W × H). DO = dissolved oxygen.

concentration of 500,000/mL without any visible residual air in the vials. Prepared vials were immediately chilled and maintained in an ice box throughout the experiment, except during treatment. This prevented the occurrence of the temperature-dependent endocytosis process during sample and experiment preparations (Khalil et al. 2006). For every independent cell viability experiment, shams were prepared alongside the treated samples. Shams captured the effect of the heated water because they were placed inside the tank for the duration of the average shock wave treatment, but were not subjected to shock wave impulses. Sample vials were treated to a combination of shock wave parameter variations: number (125, 250, 500, 1000), energy level (3, 6, 9) and pulse repetition frequency (PRF; 1, 2 Hz). All experiments were performed with the wide focal zone of the lithotripter.

mRNA and siRNA stability

Sterilised vials were filled with 1 μg/mL eGFP mRNA (StemMACS, Miltenyi Biotec, Woking, UK) in serum-free RPMI-1640 medium, in the absence of cells, and exposed to shock waves. The rabbit reticulocyte lysate cell-free gene expression system (Nuclease Treated L4960, Promega, Madison, WI, USA) was utilised to assess mRNA translation activity after shock wave treatment. The translation reaction was prepared in accordance with the supplier's protocol. Constituent volumes were adapted to the mRNA concentration as well as to permit microplate fluorometric reading, while maintaining relative proportions. A control mixture not containing any mRNA was also prepared to measure background from the rabbit reticulocyte lysate. The reactions were incubated at 37°C for 75 min. Fluorometry was then performed at 485-nm excitation and 520-nm emission.

Electrophoresis-based nucleic acid structural integrity post-shock waves was tested. Enhanced GFP (eGFP) siRNA (Silencer, Thermo Fisher Scientific) and eGFP mRNA cell-free samples were prepared at 15 and 2.5 μg/mL, respectively, in UltraPure DNAse/RNAse-free distilled water (Thermo Fisher Scientific). For siRNA analysis, traditional 1% agarose gel electrophoresis in 1× Tris–borate–EDTA buffer was performed. For mRNA analysis, the Agilent 2100 Bioanalyzer (Agilent Technologies, Palo Alto, USA) and RNA 6000 pico kit (due to low concentrated mRNA samples) were employed. The assay was conducted according to the Agilent guide for the required kit. RNaseZAP cleaning agent (R2020, Sigma-Aldrich) was applied to all equipment at the start of the procedure.

Cell survival and viability assay

Cell viability of cells was tested with the MTS assay (CellTiter 96 AQ_{ueous} One Solution Cell Proliferation Assay [3-(4,5-dimethylthiazol-2-yl)-5-(3-carboxymethoxyphenyl)-2-(4-sulfophenyl)-2*H*-tetrazolium], Promega). After exposure, 200 μL of cell suspension from each vial was plated into a 96-well plate at two wells per vial. The procedure was repeated for a second 96-well plate. Twenty microliters of MTS solution was added to each well of the first well plate and incubated for 30 min, representing the 1-h-post-exposure assay; the second well plate was incubated with the MTS after 24 h of incubation post-exposure. Absorbance was read at 490 nm (1.0-s measurement time) using a Wallac 1420 Victor^2 microplate reader (Perkin Elmer, Beaconsfield, UK).

Cell permeabilisation analysis

Membrane permeabilisation analyses were carried out using a Becton Dickinson FACSCalibur flow cytometer (BD Biosciences, Franklin Lakes, NJ, USA). Five hundred microliters of cell suspension from each vial was transferred into tubes, maintaining cells in a chilled environment. A solution of 6 μg/mL propidium iodide (PI, Sigma-Aldrich) was prepared. One hundred microliters of the solution was added to each tube, which was briefly vortexed immediately before analysis. An argon laser provided excitation at 488 nm. The software programme CellQuest Pro (BD Biosciences) was used to acquire and analyse the data. Ten thousand cells per sample were recorded and sorted by gating in two ways: (i) forward scatter/side scatter to identify viable cells, and (ii) PI staining to identify molecule-internalised cells. Data acquisition was initialised with the negative control samples, followed by all other samples in the absence of PI. The percentage of PI-positive cells was obtained by setting a gate in the PI fluorescence intensity frequency histogram of sham samples above which circa 0.1% of cells fell.

Transfection procedure

Green fluorescent protein production and knockdown were tested using eGFP mRNA and eGFP siRNA respectively. This reporter gene was selected because of its inherent stability, allowing its accumulation and easy detection in living cells (Li et al. 1998). CT26 cells at a density of 2.5×10^6/mL were employed for mRNA transfection experiments, whereas MCF-7/GFP cells at 1.5×10^6/mL were employed for siRNA transfections. Cells were immobilised in 1% w/v agar in a 2-mL custom-made tissue phantom vessel (Fig. 1b) and supplied with 5 μg mRNA or 10 μg siRNA in UltraPure DNAse/RNAse-free distilled water, before shock wave treatment. For the siRNA transfections, both the agar and the cells were prepared in Opti-MEM Reduced Serum Medium (Thermo Fisher Scientific) before mixing, whereas for mRNA transfections, cells and agar were prepared in RPMI-1640 medium and

phosphate-buffered saline, respectively. Transfection shams consisted of samples supplied with the nucleotide of interest, but not exposed to any shock wave pulses. Afterward, vessels were maintained at 37°C in cell culture incubators and removed only for analyses.

Transfections were assayed by fluorometry using the FLUOstar Omega microplate reader (BMG Labtech, Ortenberg, Germany). For mRNA transfection, fluorescence intensity (FI) was read 24 and 48 h after shock wave treatment to allow all potential cells to synthesise and express the GFP. Similarly, siRNA-mediated knockdown was assayed at 24, 48 and 72 h, a time frame defined to capture the translational arrest subsequent to target mRNA degradation. Fluorescence was visualised at the respective final assay time point using the Nikon Eclipse TiE2000 inverted microscope (Nikon, Tokyo, Japan) with a 10× objective lens; microscopic views within the upper agar region of the tissue phantom vessel were generated using NIS-Elements AR software (Nikon).

Similarly, shock wave-induced dissemination of the nucleotides across the TMM was characterised by using a eGFP mRNA analogue, fluorescein isothiocyanate-dextran (FITC-D; FD250 S, Sigma Aldrich), at a molecular weight of 250 kDa, to simulate as closely as possible the size of the eGFP mRNA (1000 nucleotides = ∼320 kDa). FITC-D was employed to determine immediate macromolecule dispersion (through spatial green fluorescence measurements), thus distinguishing shock wave-induced delivery from passive diffusion, which is time driven. A range of FITC-D amounts were tested, consisting of the mRNA dose applied in transfection, the average *in vitro* 20- to 30-μg transferred DNA amounts reported in the literature (Miller et al. 1999; Lauer et al. 1997) and a proportionally scaled up dose.

RESULTS

Influence of shock wave parameters on CT26 cell viability and permeabilisation

Expression of delivered transgenes is possible only where live cells exist. Cell response to shock waves is dependent on several factors including SW parameters, the physical environment of cells and the cell type. Shock waves can result in enhanced proliferation (Weihs et al. 2014), or marked cytotoxicity (Brümmer et al. 1989; Gambihler et al. 1990; Miller et al. 1999). Thus, shock wave-induced cytotoxicity was investigated to identify a parameter space that maximised cell viability.

Figure 2 illustrates a shock wave dose-dependent decrease in the viability of CT26 cells 1 h after exposure. This effect was greater with increasing energy level and number of shock waves, where 500 pulses at the highest attainable energy level (9 E) amounted to a viability of

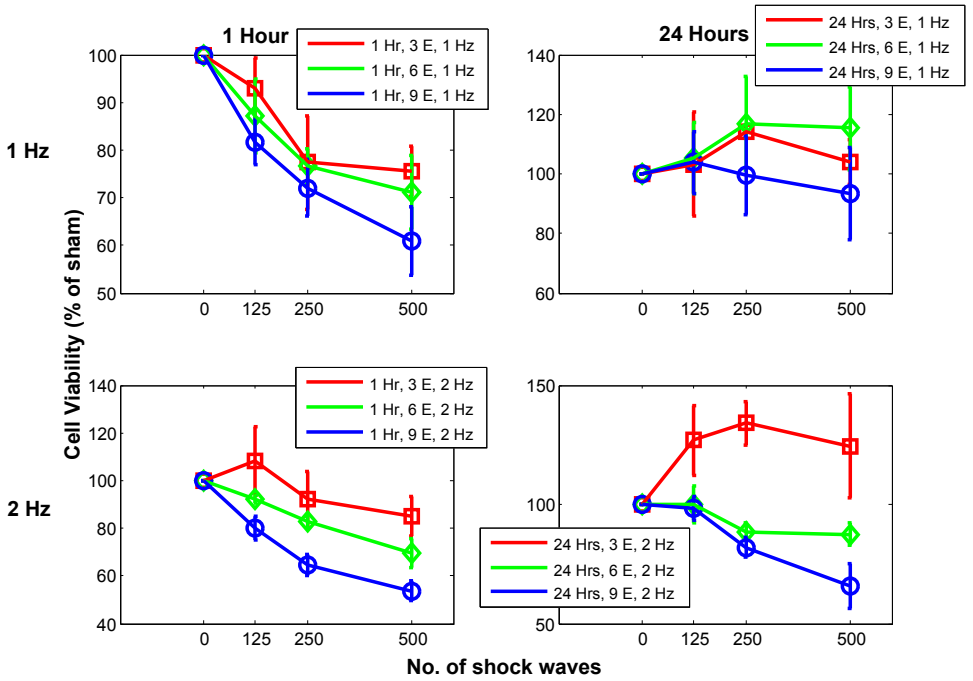

Fig. 2. Influence of shock wave exposure on cell viability. CT26 cells were assayed at 1 or 24 h after exposure using the MTS (3-(4,5-dimethylthiazol-2-yl)-5-(3-carboxymethoxyphenyl)-2-(4-sulfophenyl)-2*H*-tetrazolium) assay. The influence of number of shock waves, energy and pulse repetition frequency was investigated. Data points represent the mean values of three same-day replicates per treatment, for at least three separate-day experiments (*i.e.*, n = 9). Error bars are standard errors.

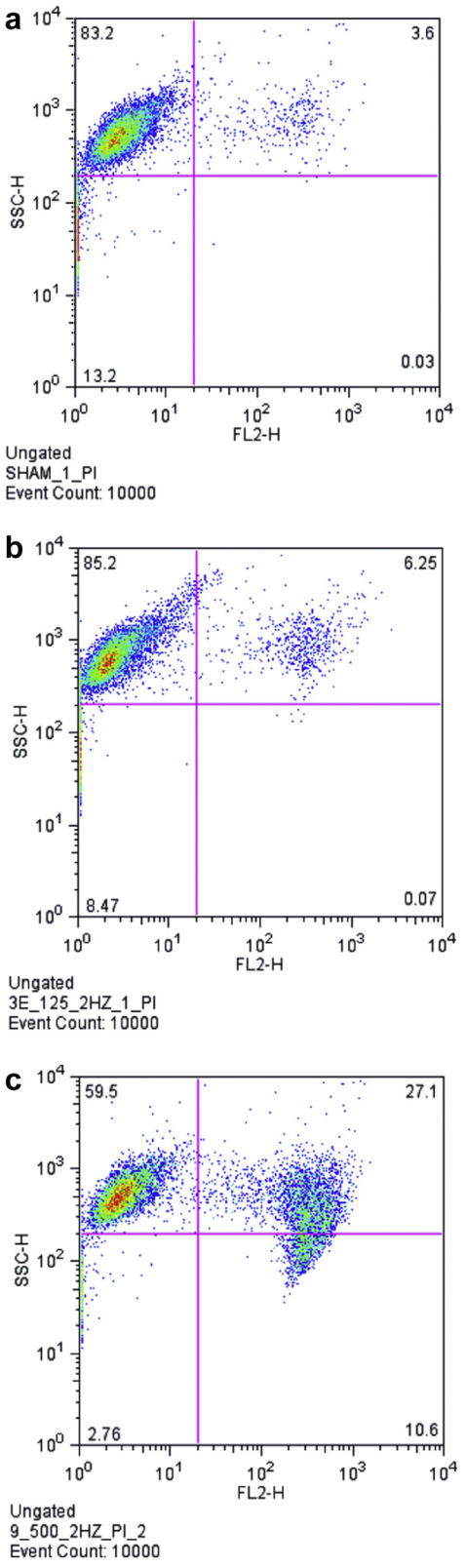

Fig. 3. Flow cytometric measurements of CT26 cell permeabilisation and viability. Cell permeabilisation was assessed through propidium iodide (PI) fluorescence-assisted cell sorting (using the FL2-H channel for PI fluorochrome detection), and viability was analysed through forward (FSC) and side (SSC) scatter. Density plots illustrate representative cell populations for three treatments: sham (a); 3 E, 125 pulses, 2 Hz (b); 9 E, 500 pulses, 2 Hz (c). The fluorescence-based quadrant gates (*purple lines*) were set to identify the percentage of PI-positive intact events. The data are representative of nine repeats.

50%–60%. Varying the PRF from 1 to 2 Hz did not alter the overall pattern of this loss of viability. At 24 h, MTS assays were performed again, and comparison with 1-h data allowed the recovery of cells to be characterised. The 24-h viabilities were comparably elevated in the majority of cases, indicating a population growth phase at or within 24 h. However, the extent of growth differed between treatments as well as within treatment replicates, with some treatments (*e.g.,* 3 E, 250 pulses, 2 Hz) suggesting metabolic activity within the wells was doubling between the 1- and 24-h readings; other treatments (*e.g.,* 9 E, 500, 2 Hz) caused minimal sustained depletion of viability, implying that under those conditions, shock waves instigated damage from which the cells could not recover. The shock wave stimulative effect at low energy was evidenced at both PRFs in the 24-h assay; a wider range of energies displayed this effect at 1 Hz, whereas proliferation peaked at 2 Hz.

The impact of shock waves on cell viability was probed further using flow cytometry (*recall* methods). Figure 3 provides example distributions for a sham-treated population (a), a minimally exposed (3 E, 125 shocks, 2 Hz) population (b) and a maximally exposed (9 E, 500 shocks, 2 Hz) population (c). Based on the untreated (sham) cells, subpopulations such as fragmented cells and cellular debris were identified by side scatter (SSC), which is proportional to cell granularity. Cell permeabilisation, as characterised by cell staining with PI immediately after shock wave exposure, was quantified by the fluorescence gate separating the SSC/FL2-H plots into left and right halves, as illustrated in Figure 3 (where FL2 is a channel for the detection of emission wavelengths comprising the emission peak of PI). Events in the right half represented the proportion of total PI-positive cells, which is seen to increase with increasing shock wave parameter.

The minimum SSC of the untreated population provided a baseline for an additional gate to separate intact from damaged cells, where the first quadrant identifies the population of whole and permeabilised cells. Note that less than 4% of cells were intact and PI-positive in the sham samples, suggesting that a small proportion of cells became compromised by the removal of culture conditions. Reversible damage (*i.e.,* transiently permeabilised cells) was determined by correlating total

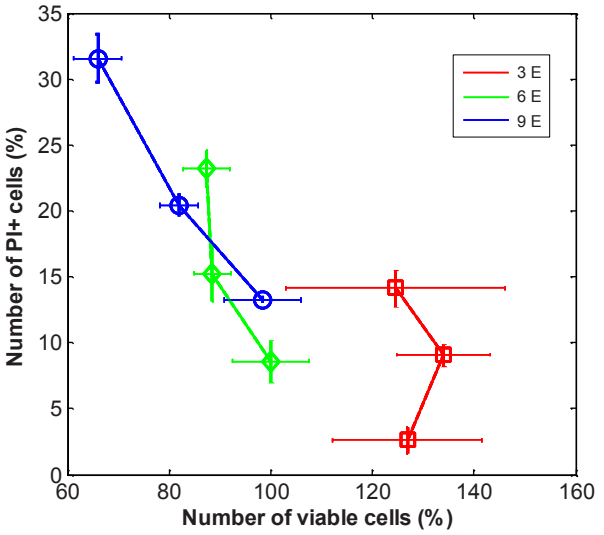

Fig. 4. CT26 cell permeabilisation combined with results of 24-h viability. Data points represent the means of three same-day replicates, for at least three separate-day experiments (*i.e.,* n = 9). Error bars are the standard errors. PI = Propidium iodide.

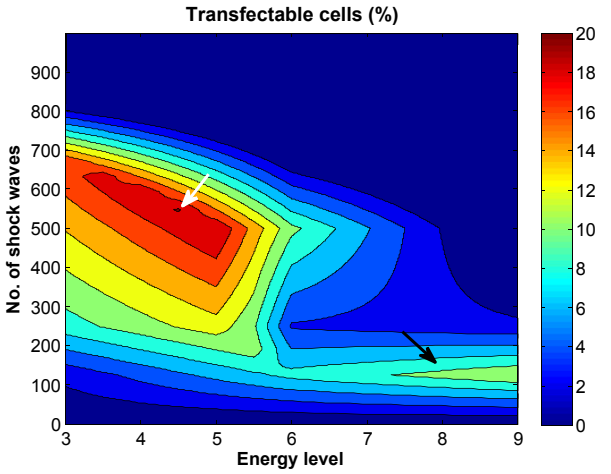

Fig. 5. Transfectability of CT26 cells as a function of the number of shock pulses (0–1000) and energy level (3–9) at 2 Hz. Transfectability is defined as the percentage of live permeabilised cells. Three independently conducted experiments at 1000 pulses, with three same-day replicates at each tested energy level, were included.

PI-positive cells with the 24-h viabilities. In so doing, a parameter space defined by 9 E, 125, 2 Hz and 3 E, 500, 2 Hz was found that permitted temporal membrane permeabilisation to the PI of up to ∼15%, without any associated cell death (Fig. 4). For almost all shock wave conditions, results revealed an inverse correlation between the percentage of permeabilised cells and viability.

The influence of PRF on cell viability was further investigated, to a maximum of 4 Hz, which could only be realised for energy levels 3 and 9 (data not shown) because of the capacitance of the shock wave source. For a fixed number of shock waves (250), while varying the PRF in increments of 1 Hz, no statistical significance was found between PRFs in both energy level sets (p = 0.8 and 0.49 for the 3 E and 6 E sets, respectively). Thus, it was thought that for any two treatments where only the PRF was the varying parameter, any difference in apparent viability was due to changes in cell morphology (*i.e.,* cell injury) rather than cell destruction, because of PRF-effectuated cell accelerations and/or collisions.

Optimisation of shock wave parameters

The shock wave settings that imparted the maximum number of permeabilised (as detected by PI staining) but still viable (as detected by MTS) cells was sought. This value may be considered the "transfectable" population. Although all killed cells are permeabilised, not all permeabilised cells are killed. A 2-D interpolation of CT26 cell permeabilisation and 24-h viability was performed between data points, in increments that related to attainable lithotripter settings, and the proportions of permeabilised cells above the proportions of non-viable cells were derived. Figure 5 illustrates the resulting contours of high and low transfection power across shock wave energies and numbers of pulses. The highest value is seen to be produced by 548 shock waves, at 4.5 E (see *white arrow*), where 20.19% of total cells are theoretically capable of being transfected in the presence of a nucleic acid, whilst maintaining 24-h cell survival rates at 100%. To confirm this effect, the optimum shock wave setting was experimentally tested, and a reversible cell permeabilisation of 20.5 ± 2.7% was found. Karshafian et al. (2009) optimised their ultrasound exposure system by deriving a similar measure that compared the desired and destructive effects of any given shock wave condition.

Notably, Figure 5 also illustrates that at the highest energies and circa 150 pulses (see *black arrow*), there is a local increase in the percentage of live permeabilised cells, suggesting that a regime consisting of a few shock waves at high peak pressures may exist where appreciable cell permeabilisation is attained.

Shock wave pressure

In Figure 6(a) are pressure waveforms measured at the focus of the lithotripter at the optimal energy level for CT26 cells, in degassed water and with the needle hydrophone in the polypropylene vial. The presence of the vial decreased the peak positive pressure by 57% and increased the duration of the compressive phase from 2.57 to 4.63 μs, which was measured from the

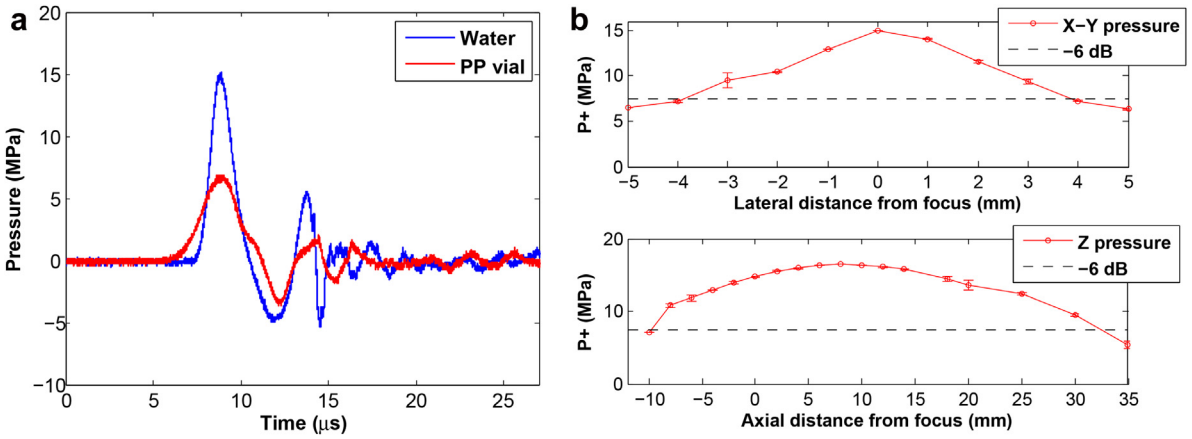

Fig. 6. (a) Representative shock waveform at energy level 4.5 when measured at the focal point in degassed water and inside the polypropylene vial. (b) Measurements of peak positive pressure at energy level 4.5, in the direction perpendicular to the shock wave propagation path (x–y) and along the path (z). Error bars are standard deviations (range: 0.07–0.86 MPa). The focal zone is marked by the *dashed line* representing the pressure being 6 dB less than the maximum peak positive pressure.

positive pressure that first exceeds 10% of the peak positive pressure, up to the first time the positive pressure decreases below 10% of the peak positive pressure (International Electrotechnical Commission 1998). The negative pressure did not change substantially, as evidenced by a 1.3-MPa decrease when inside the vial, either as a result of the limiting hydrophone's susceptibility to damage, stemming from cavitation during the negative phase (Smith et al. 2012), or because the negative phase is more sensitive to the low-frequency components of the signal and thus less affected by the vial. Moreover, the presence of the vial did not appreciably change the shape of the waveform. At the focal point, the peak pressures for energy levels 3, 4.5, 6 and 9 are given in Table 1.

The variation in peak positive pressure in the focal zone of the lithotripter at energy level 4.5 was also measured. Figure 6(b) illustrates peak pressure in the lateral plane (x, y) and along the propagation path (z). The maximum error in hydrophone positioning was a standard deviation of 0.86 MPa. In the lateral direction the pressure amplitude dropped to 50% as demarcated by the −6-dB threshold line, at a radial distance of 3.9 mm, whereas in the axial direction, the −6-dB focal zone was asymmetric about the focus and spanned 42.4 mm. Therefore, the incident pressure field was relatively uniform within the exposure vessels (vial and TMM were 9 or 10 mm wide and 40 mm long), although the vessel material is likely to have resulted in some variation.

Table 1. Shock wave focal pressure

Energy level	Peak positive (MPa)	Peak negative (MPa)
3 E	8.6 ± 0.3	4.7 ± 0.3
4.5 E	14.9 ± 0.2	5.0 ± 0.1
6 E	20.7 ± 0.8	6.4 ± 0.4
9 E	37.0 ± 0.5	7.2 ± 0.5

Permeabilisation and viability of HK-2 and MCF-7/GFP cells

The impact of shock waves on other cell lines was investigated using HK-2 and MCF-7 cells to gauge variability across different cell types. Cell permeabilisation and viability data were processed similarly to data from CT26 cells. Appropriate settings for the flow cytometer's detectors and amplifiers were adjusted accordingly. However, for MCF-7/GFP cells, PI positivity was detected using the FL3 channel because of the GFP signal bleeding into the FL2 channel. The overlap between FL2 and FL3 detectors at 620 nm enabled PI detection in either channel.

The cell viabilities of HK-2 cells were shock wave dose dependent, with values ranging from ∼70% to ∼129% relative to sham controls. In contrast, the permeabilisation of HK-2 cells (Fig. 7) revealed little correlation with shock wave parameters. However, a measurable level of shock wave-induced permeabilisation was observed, highlighting the sensitivity of the cell line to ultrasound. Given that HK-2 cells are transformed, rather than of cancer origin, provides evidence of shock wave applicability in non-cancerous gene therapy applications.

Results of MCF-7/GFP permeabilisation, illustrated in Figure 7, confirmed the differential effect of shock waves on cancer cells, previously observed with

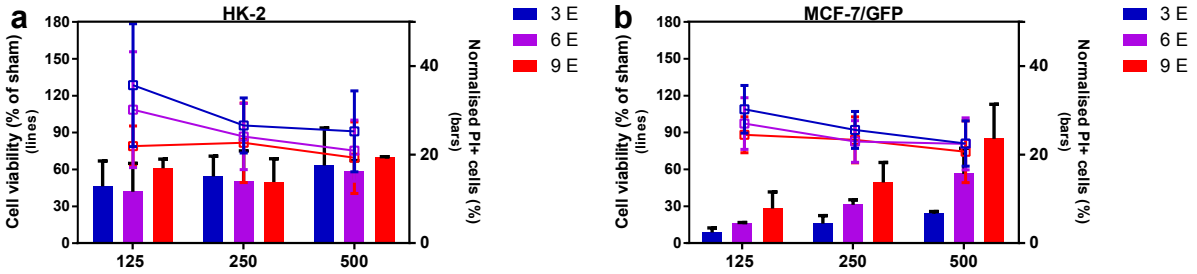

Fig. 7. Influence of shock wave exposure on HK-2 and MCF-7/GFP cell permeabilisation (*bars*) and 24-h-post-exposure cell viability (*lines*). Data points represent the mean values of three same-day replicates per treatment, for three separate-day experiments (*i.e.,* n = 9). Error bars are standard deviations. HK-2 = immortalised human proximal tubule epithelial cells; MCF-7/GFP = human breast cancer cells stably expressing green fluorescent protein; PI = propidium iodide.

CT26 cells, where both shock wave energy and number of pulses were effective discriminants. However, the cell line revealed reduced amenability to be efficiently transfected as the highest proportion of permeabilised cells above that of killed cells was found to be 4.1% by exposure to 134 shock waves, energy level 5.0, at 2 Hz. Although up to 23.5% of cells could be permeabilised (500 shocks, 9 E), these parameters were associated with a 25% loss in viability. This is consistent with reports that have described MCF-7 cells as "hard to transfect" in the literature (Fire et al. 2005).

RNA stability

Having identified shock wave parameters that would allow transfection whilst maintaining cell viability, the effect of shock waves on the stability of nucleotide was tested. The structural stabilities of mRNA and siRNA were determined using the Bioanalyzer and traditional gel electrophoresis respectively. Figure 8(a-1) depicts representative electropherograms of sham and optimum shock wave treated mRNA. The distinct 18 S and 28 S ribosomal peaks of typical RNA were present in both treatments. No shift in nucleotide (nt) size of both peaks was observed with optimal shock wave exposure. In

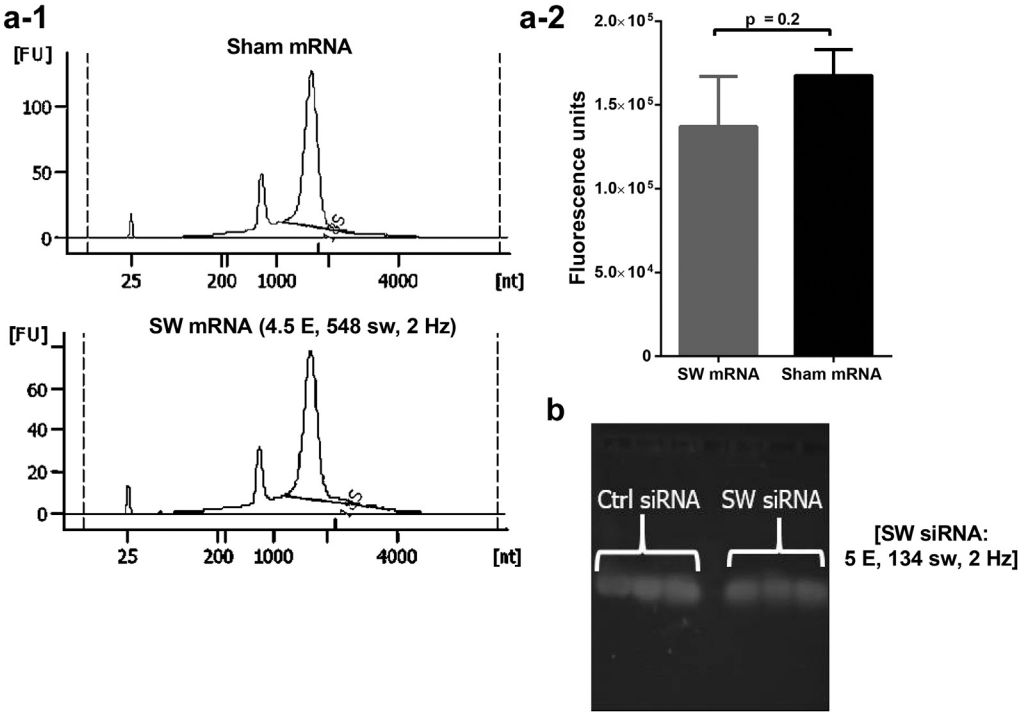

Fig. 8. Results of stability post shock wave exposure for (a) mRNA and (b) siRNA, compared to sham controls. Structural stability data depict (a-1) representative mRNA electrophoretic profiles and (b) agarose gel electrophoresis for siRNA analysis (based on n = 3), and (a-2) mRNA biological activity data consisting of one sample per treatment, for three independently conducted experiments (n = 3). Error bars represent the standard deviations. FU = fluorescence units; siRNA = small interfering RNA; SW = shock wave.

addition, the absence of smaller peaks between the two ribosomal peaks (typically observed in partially digested RNA) suggested that the structure-based functionality of the exposed mRNA had not been impaired. However, a 22% decrease in the 28 S ribosomal peak intensity was detected with shock wave exposure (1765 ± 183 pg/μL for the shams vs. 1363 ± 115 pg/μL for the shock wave treated, based on n = 3). On the stability of siRNA, Figure 8(b) illustrates that optimal shock waves for MCF-7/GFP cells did not substantially affect the structure or concentration of siRNA, with comparably equal migration and similar fluorescence intensity of the bands with respect to the non-shocked siRNA.

Maintenance of mRNA biological stability was assayed by performing cell-free protein translations of the GFP mRNA transcript, allowing for absolute measurements of shock wave-induced damage to the activity of the mRNA, as there was no cell interference during exposure. Figure 8(a-2) illustrates the translational activity of sham controls and optimum shock wave-treated samples, in terms of GFP fluorescence intensity. An 18% drop in mean fluorescence intensity was observed between sham and optimum shock waves (167,570 vs. 137,125 fluorescence units, respectively) which was not found to be statistically significant. Thus, results from both stability methods were in agreement on the effects impacted onto the mRNA by shock waves. Though there are no previous direct investigations of the (in)stability of mRNA in acoustic fields, Forbrich et al. (2013) reported ultrasound-enhanced cellular liberation of endogenous mRNA. They determined significant numbers of liberated mRNA molecules, as assayed by reverse transcription and quantitative polymerase chain reaction, thus entailing functional post-exposure mRNA. Furthermore, although ultrasound-assisted delivery of complexed mRNA has been reported (De Temmerman et al. 2011), no comparison can be made between free and complexed mRNA.

Ultimately, the reported reduction in RNA quality caused by shock waves was found to be slight and non-significant compared with the potential for enhanced nucleotide delivery.

Shock wave-mediated dissemination of 250-kDa FITC-D in agar is a function of macromolecule availability

The application of shock waves has the added potential to improve the transfer of nucleotide from blood vessels and into target tissue. Having identified shock wave exposure conditions that were conducive to cell viability and maintenance of nucleotide structure, the impact of these conditions on mass transfer out of a model channel and into the TMM was investigated. Using the custom-made tissue phantom vessels (see Fig. 1b), FITC-D was loaded into the vessel (0 mm), exposed to shock waves from beneath and transfer toward the shock wave source (up to −20 mm) or away from the shock wave source (up to +20 mm) was measured.

Figure 9 depicts results of scaled fluorescence against distance below (−2.5 to −20 mm) and above (2.5 to 20 mm) the channel. The channel is illustratively demarcated by the *dash-dot lines*. At all three dextran amounts (*red line*), there was an elevated fluorescence signal in the upper agar region (between +2.5 mm and +20 mm) in the presence of shock waves, as compared with the sham treated samples (*blue line*). At the farthest distance (20 mm), scaled intensities were ∼ 6-, 8- and 25-fold higher than corresponding sham intensities at 5, 30 and 180 μg FITC-D respectively. Contrast between shams revealed some degree of passive dissemination into the agar from the channel, where increasing dextran mass increased the fluorescence in the vicinity of the channel.

GFP mRNA transfection

Experiments were performed to investigate if cells embedded in TMM could produce transgene from nucleotide delivered through a channel compartment within the TMM. Cells were transfected with eGFP mRNA in the absence and presence of the optimal shock waves and incubated for periods of 24 and 48 h. For fluorescence reading, the 40 × 10 × 5-mm Mylar window was discretised into 1 × 1 × 5-mm volumes, and fluorescence values were recorded for each. Due to cell growth and/or migration, the calculated mean FIs included the channel regions as well. Figure 10(a) illustrates the levels of GFP expression at the two time points for both sample treatments. The fluorescence of no-treatment samples comprising only cells was subtracted from the recorded FIs of the shock wave- and sham-treated samples. For a given independently conducted experiment, the FI variance between replicates was generally higher at 24 h than at 48 h, which was thought to be due to time differences in the onset of protein synthesis. Low numbers of successfully transferred nucleic acids have been previously attributed to the often observed stochasticity in gene expression (Schwake et al. 2010).

At 24 h after shock wave exposure or sham treatment, the FI of shock wave-treated cells, compared with shams was substantially ∼6-fold higher. When cells were incubated for a further 24 h, an ∼52-fold increase ($p < 0.05$) in FI was evident for the shock wave-treated cells. FI levels could not be correlated with the number of GFP-positive cells, because of the multiplanar presence of cells in deep tissue phantom samples, as well as the GFP spatial heterogeneity observed microscopically (see Fig. 10b). The images represent 835.2 × 624-μm areas (0.6 μm/px at 1392 × 1040),

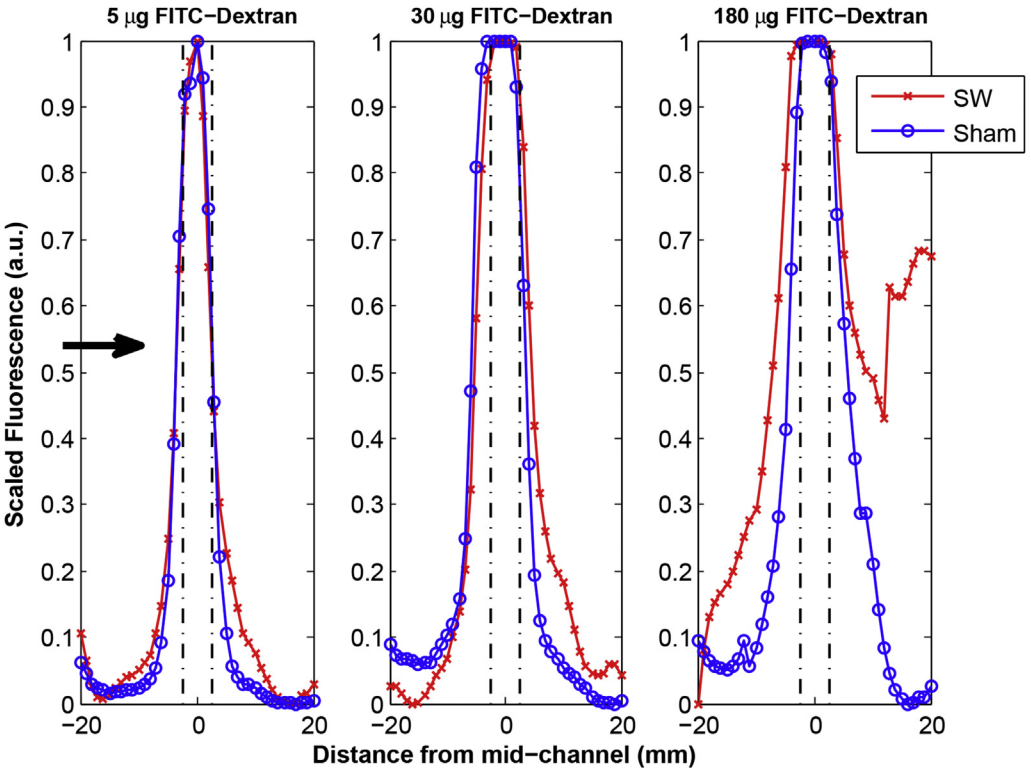

Fig. 9. Representative disseminations of 250-kDa fluorescein isothiocyanate (FITC)-dextran within the TMM, along the direction of shock wave propagation (*i.e.,* from −20 to 20 mm) after shock wave or sham treatment. The areas in-between the *dash-dot lines* represent the channel width. The *black arrow* indicates the direction of shock wave propagation.

depicting intensely green fluorescent cells when exposed to the optimum shock waves. In contrast, little GFP signal could be detected microscopically in the sham samples. RNA transfection promotes transient gene expression; hence, strongly expressing cells are desirable to produce sufficient therapeutic benefit.

GFP siRNA transfection

In addition to providing production of therapeutic protein, the tissue-mimicking phantom developed here was tested to see if the delivery of siRNA could be achieved to provide knockdown of a GFP reporter gene. An initial assessment was performed on fluorescence quantification for four MCF-7/GFP concentrations over a 4 log range, and a linear relationship was found between FI and cell concentration, indicating the ability of the quantification method to detect small changes in the number of fluorescent cells.

Results of shock wave–mediated GFP knockdown are illustrated in Figure 11(a). For siRNA delivery, the optimal shock waves for MCF-7/GFP cells were delivered to samples. Three forms of negative control were tested: (i) gene knockdown specificity (using scrambled siRNA whose sequence is intentionally non-complementary to that of the mRNA encoding GFP); (ii) sham treatment; and (iii) no treatment (absence of both GFP siRNA and shock wave exposure). An additional no-treatment control based on non-GFP MCF-7 cells was tested to distinguish between GFP and autofluorescence detection. For all samples, the region of analysis was restricted to the agar area 5 mm above the channel, in which a differential effect between treatments was observed.

Comparisons of relative fluorescence between treatment groups using one-way analysis of variance revealed statistical significance at all three time points ($p < 0.05$). The maximum depletion of GFP signal occurred at 48 h in cells exposed to siRNA and shock waves. This result was 17% higher than that for sham controls. The largest difference in GFP fluorescence (∼23%) between sham and siRNA + shock waves was recorded at 72 h. Figure 11(b) compares the spatial fluorescence across the TMM between siRNA/+ SWs and sham siRNA. GFP reduction was also observed in all three negative controls with a peak loss of ∼5% relative to sham, occurring in the scrambled siRNA + SWs samples, implying a small percentage of shock wave-induced cell death at 72 h. The FI decrease over time was generally invariable

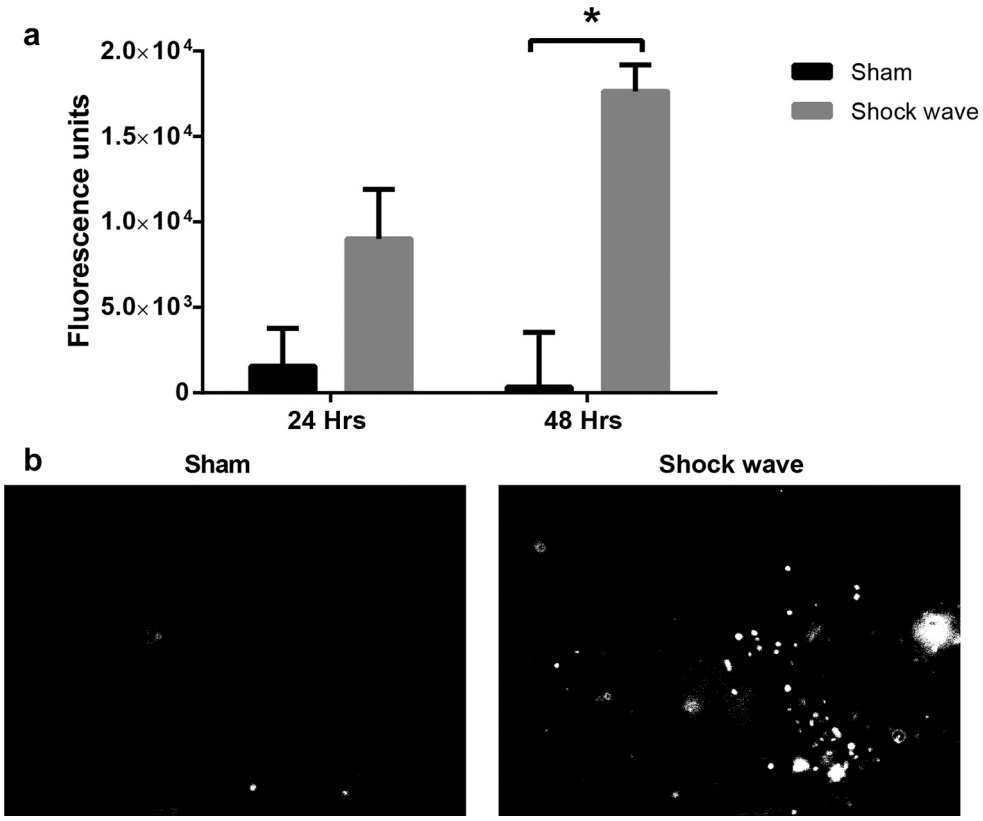

Fig. 10. Results of enhanced green fluorescent protein mRNA delivery to CT26 cells for shock wave- and sham-treated samples. (a) Data are expressed as the means of intensities of six replicates per sample across two independently conducted experiments. Error bars are standard deviations. Significance was tested using the two-tailed unpaired parametric *t*-test where $*p < 0.05$ ($p = 0.04$). (b) Representative images of green fluorescent protein expression at 48 h after sham or shock wave treatment. Images were converted to binary by thresholding.

between negative controls, suggesting a degree of cytotoxicity to affect MCF-7 cells exposed to the TMM *in vitro* system for over 24 h. Furthermore, at 72 h, an increase in fluorescence was observed in all groups, but particularly in the nucleotide-containing treatments. Two possible reasons for the slight fluorescence recovery are as follows: (i) non-GFP MCF-7 cells (data not shown) revealed an upward trend in cellular fluorescence with increasing time, to a maximum of 12% relative to the initial (background) fluorescence read at 0 h. Such autofluorescence, which is indicative of cell necrosis and increases with decreasing metabolic activity, may have explained the upturn of fluorescence at 72 h. (ii) Cell proliferation up to 72 h was likely to have produced the increased GFP signal because of an increase in the number of cells. In the case of the siRNA + SW treatment, the net increase in fluorescence was due to a concurrent loss of siRNA function resulting from its degradation (of which 72 h defines a time well beyond its onset, considering siRNA's half-life of 24 h [Bartlett and Davis 2006]).

Post hoc pairwise comparisons using the Tukey range test did not prove statistical significance for scrambled siRNA or no-treatment results, compared with sham siRNA, at any time point analysed. However, significant differences were detected between siRNA + SWs and sham siRNA: $q = 7.08 > q(\text{crit} = 6.35)$, $q = 17.12 > q(\text{crit} = 13.67)$, $q = 23.2 > q(\text{crit} = 19.8)$ at 24, 48 and 72 h respectively]. At 48 h, the difference between the two shock wave (+SW) groups was found to be significant, signifying treatment specificity as well as enabling separation of the proportion of siRNA silenced GFP cells from those collaterally silenced as a result of shock wave-induced damage.

DISCUSSION

Externally applied ultrasound offers an increasingly popular approach to tackling the challenge of gene delivery (Carlisle et al. 2013). Shock wave exposure may be particularly attractive in certain situations because it is comparatively low cost, clinically available and has a safety track record through lithotripsy. The presented studies indicated that exposure of cancer cell lines *in vitro* to lithotripter shock waves, using clinically

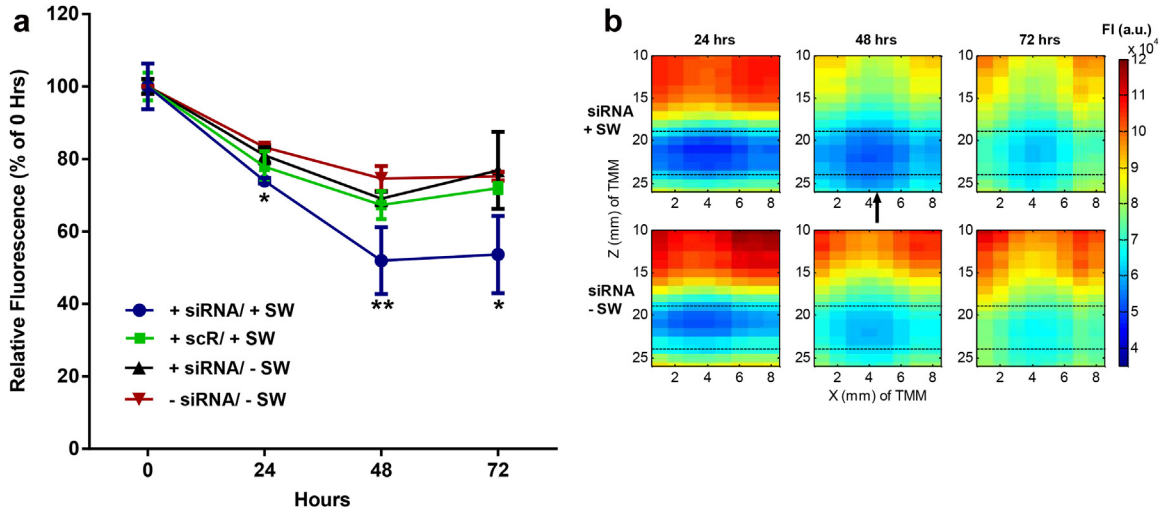

Fig. 11. Results of anti-eGFP siRNA delivery to MCF-7/GFP cells. (a) GFP intensities of shock wave treated (+SW) and non-treated (−SW) samples consisting of three replicates per sample for one independently conducted experiment, up to 3 d after sample preparation or treatment. Data are expressed as the percentage fluorescence relative to initial fluorescence. Error bars are standard deviations. Significance was tested using one-way analysis of variance and *post hoc* Tukey range tests. The latter revealed statistical significance, denoted by the asterisks: *between siRNA + SW and sham; **between siRNA + SW and scR + SW, in addition to (*). (b) Representative spatial fluorescence intensities across the TMM region of interest for SW and sham siRNA treatments; the *dashed lines* demarcate the siRNA-incorporated channel. The *black arrow* represents the direction of SW propagation. eGFP = enhanced green fluorescent protein; FI = fluorescence intensity; siRNA = small interfering RNA; scR = scrambled RNA; TMM = tissue-mimicking material.

available parameter settings, resulted in differential cell viability and reversible membrane permeabilisation.

In the mouse colorectal carcinoma cell line, the acquired cell viability data revealed high statistical power ($p < 0.01$) between 125, 250 and 500 pulse number sets (encompassing the various energy levels and PRFs tested). In fact, microscopic examination revealed that doubling the number of pulses produced progressively shrunken cells in the presence of some cellular debris. In human breast cancer cells, comparably more irreversible permeabilisation was noted, as reflected by the poor recovery of viability at 24 h (Fig. 7b).

A study by Guck et al. (2005) on the elasticity of MCF-7 cells, based on an optical stretching technique, revealed an approximate 10% increase in peak deformability compared with other malignant cells. We speculate that the lower elasticity of MCF-7 cells resulted in greater deformation when subjected to shock waves, hence producing greater damage and permeabilisation. On the other hand, cell viability data for the transformed non-cancerous human kidney cells revealed a sensitivity to shock waves comparable to that of CT26 cells. Brümmer et al. (1990) made a similar conclusion regarding malignant and normal cells as they found no significant difference in their median lethal dose (LD_{50}) values. Although HK-2 manifests both normal and cancerous cell characteristics, these non-malignant cells further agreed with the non-distinguishing dose effect of normal cells observed by Brümmer et al. (1990) because uniquely high cell permeabilisation levels could not be established.

Shock wave parametric studies were conducted to determine the settings that maximised cell permeabilisation with no effect on the viability. The optimal number of pulses for MCF-7 cells was four times less than the number required for CT26 cells, whereas the similarity in optimal shock wave energy indicated the presence of an energy threshold below which reversible permeabilisation is negligible.

Sonoporation is a process of temporary benefit, as the cell membrane naturally re-forms afterward if the cell remains viable. The time taken for such repair has not been defined for most cell lines, and there are few data concerning the differences between cancer cell lines and primary cells. The ability of transiently defected cells to permit PI entry was characterised as a measure of permeabilisation. PI is a nuclear stain that is detected upon binding to cellular DNA. Therefore, PI is a late marker in the context of plasma membrane permeability and excludes the population of cells whose nuclear membrane is intact but whose plasma membrane is compromised. It follows that our reversible plasma membrane permeabilisation results of 20.5% and 4.1% for CT26 and MCF-7 cells, respectively, are underestimates of the proportion of potentially RNA transfectable cells, as these require only perturbation of the plasma membrane.

Results comparable to those for CT26 transfectability have been obtained using therapeutic ultrasound (centre frequencies of 1–5 MHz) and variable intensity levels, where 28% (Duvshani-Eshet et al. 2005) and 32% (Karshafian et al. 2009) transfected or transfectable cells, respectively, have been reported per total number of cells. However, the latter was attained in the presence of ultrasound contrast agents to function as nuclei for cavitation. Our shock wave-mediated transfection required no nucleation agents.

Experiments were designed by considering a number of aspects that would affect shock wave propagation to the cells and gene delivery efficiency. First, the shock wave-induced cell streaming in fluid at low cell concentrations and subsequent reduced bio-effects inspired the development of TMM exposure vessels (Fig. 1b) that permitted the analysis of immobilised cells without needing to dislodge them. Cells embedded in agar allowed shock wave forces to act directly on the cells, thus more likely reflecting the transfection levels that may be observed in tissue, than experiments using isolated cells in solution. Second, preliminary transfection tests revealed that the cell or nucleotide concentrations were not as important as the cell-to-RNA ratio (data not shown). A supporting study by Bao et al. (1998) scaled up *in vitro* mRNA dose for *in vivo* use and obtained lower transfection efficiencies *in vivo* than they had *in vitro*, probably because the assumed cell-to-mRNA ratio may not have applied to both conditions. In our transfections, the lowest nucleotide concentrations that produced a measurable and distinguishable transfection effect between treatments were employed. At an equivalent dose (*i.e.,* 5 μg), RNA-like penetration in 1% agar with optimal shock waves resulted in a maximum distance travelled of approximately 10 mm above the channel, whereas greater depths were attained with increasing availability of the macromolecule (Fig. 9). However, the study was limited by FITC-D emissions in areas where GFP mRNA expression cannot take place, such as on cell membranes.

In this work *in vitro* transfections were performed in a new tissue-mimicking model, that is, not suspended in cell culture or growth medium, but having compartmentalised RNA and cells, in an effort to simulate nucleic acid administration *via* the bloodstream. As such, the efficiency of gene delivery could not be assessed in a single-cell fashion, and thus, the number of transfected cells is not given. Notably, this SW exposure system allowed us to report considerable mediation in gene augmentation and gene knockdown with optimal lithotripter shock wave treatment, compared with sham treatment. In comparison to the similarly low concentrations of nucleotide (plasmid DNA) administered (1–5 μg in 10^6 cells), Huber et al. (1999) reported that only 800 of one million cells were successfully transfected, whereas Murata et al. (2007) reported a less than twofold increase in luciferase expression, relative to control with shock wave application. In this first study, to our knowledge, of shock wave-assisted mRNA delivery, an enhancement greater than 50-fold was attained. Furthermore, siRNA transfection was enhanced with optimal shock wave exposure despite being challenged by the cell line's relatively low amenability to delivery, with a twofold increase in knockdown relative to sham siRNA at 72 h being achieved. Similarly, Ha et al. (2015) transfected CT26 cells with anti-GAPDH siRNA through low energy shock wave exposure and obtained an approximately threefold decrease in the relative GAPDH expression compared with controls in an *in vitro* setup comprising a shock wave probe immersed in cell suspensions. In the presence of microbubble contrast agents and unfocused ultrasound in lieu of shock waves, Juffermans et al. (2014) reported an approximately fourfold decrease in GAPDH expression.

CONCLUSIONS

We found that shock wave exposure can successfully induce RNA transfer into cells without imparting cellular or nucleic acid damage and that this may be possible in a broad range of tissue types by tuning the shock wave exposure parameters. These effects were accomplished using a clinical electromagnetic lithotripter, which provides a pathway for clinical translation. Variability in the optimum parameters is expected where different types of lithotripters (*e.g.,* piezoelectric, electrohydraulic) are employed, having a dissimilar focal volume and shock waveform from those in this work. Further research is to be undertaken to determine how these findings may affect therapy and its effectiveness.

Acknowledgments—S. Nwokeoha acknowledges support under Research Councils UK (RCUK) Digital Economy Programme Grant EP/G036861/1 (Oxford Centre for Doctoral Training in Healthcare Innovation). R. Carlisle and R. Cleveland are supported by Engineering and Physical Sciences Research Council (EPSRC) under Programme Grant EP/L024012/1 (OxCD3: Oxford Centre for Drug Delivery Devices).—The authors thank James Fisk and David Salisbury for the manufacture of the custom tissue phantom vessels and holders. We are also grateful to Ben Turney and Mandy Spencer, Oxford Stone Group at Churchill Hospital, Oxford, for providing access to the Storz lithotripter for our experiments. Finally, we thank Fiona Yi Lee, Department of Physiology, Anatomy and Genetics (University of Oxford), for access to and training on the Bioanalyzer.

REFERENCES

Bao S, Thrall BD, Gies RA, Miller DL. In vivo transfection of melanoma cells by lithotripter shock waves. Cancer Res 1998;58:219–221.

Bartlett DW, Davis ME. Insights into the kinetics of siRNA-mediated gene silencing from live-cell and live-animal bioluminescent imaging. Nucleic Acids Res 2006;34:322–333.

Ben-Dor G, Igra O, Elperin T. Handbook of shock waves. San Diego: Academic Press; 2000.

Bertrand JR, Pottier M, Vekris A, Opolon P, Maksimenko A, Malvy C. Comparison of antisense oligonucleotides and siRNAs in cell culture and in vivo. Biochem Biophys Res Commun 2002;296:1000–1004.
Bettinger T, Carlisle RC, Read ML, Ogris M, Seymour LW. Peptide-mediated RNA delivery: A novel approach for enhanced transfection of primary and post-mitotic cells. Nucleic Acids Res 2001;29:3882–3891.
Brümmer F, Bräuner T, Hülser DF. Biological effects of shock waves. World J Urol 1990;8:224–232.
Brümmer F, Brenner J, Bräuner T, Hülser DF. Effect of shock waves on suspended and immobilized L1210 cells. Ultrasound Med Biol 1989;15:229–239.
Carlisle R, Choi J, Bazan-Peregrino M, Laga R, Subr V, Kostka L, Ulbrich K, Coussios CC, Seymour LW. Enhanced tumor uptake and penetration of virotherapy using polymer stealthing and focused ultrasound. J Natl Cancer Inst 2013;105:1701–1710.
Chaussy C, Brendel W, Schmiedt E. Extracorporeally induced destruction of kidney stones by shock waves. Lancet 1980;316:1265–1268.
Cleveland RO, McAteer JA. The physics of shock wave lithotripsy. In: Smith AD, Badlani G, Bagley D, (eds). Smith's textbook of endourology, 1. Hamilton, ON: Decker; 2007. p. 529–558.
De Temmerman ML, Dewitte H, Vandenbroucke RE, Lucas B, Libert C, Demeester J, De Smedt SC, Lentacker I, Rejman J. mRNA-lipoplex loaded microbubble contrast agents for ultrasound-assisted transfection of dendritic cells. Biomaterials 2011;32:9128–9135.
Delius M, Adams G. Shock wave permeabilization with ribosome inactivating proteins: A new approach to tumor therapy. Cancer Res 1999;59:5227–5232.
Duvshani-Eshet M, Baruch L, Kesselman E, Shimoni E, Machluf M. Therapeutic ultrasound-mediated DNA to cell and nucleus: Bioeffects revealed by confocal and atomic force microscopy. Gene Ther 2005;13:163–172.
Fire A, Nirenberg M, Appasani K. RNA interference technology: From basic science to drug development. London/New York: Cambridge University Press; 2005.
Forbrich A, Paproski R, Hitt M, Zemp R. Microbubble-enhanced ultrasound liberation of mRNA biomarkers in vitro. Ultrasound Med Biol 2013;39:1087–1093.
Gambihler S, Delhis M, Ellwart J. Permeabilization of the plasma membrane of L1210 mouse leukemia cells using lithotripter shock waves. J Membrane Biol 1994;141:267–275.
Gambihler S, Delius M, Brendel W. Biological effects of shock waves: Cell disruption, viability, and proliferation of L1210 cells exposed to shock waves in vitro. Ultrasound Med Biol 1990;16:587–594.
Gilboa E, Vieweg J. Cancer immunotherapy with mRNA-transfected dendritic cells. Immunol Rev 2004;199:251–263.
Guck J, Schinkinger S, Lincoln B, Wottawah F, Ebert S, Romeyke M, Lenz D, Erickson HM, Ananthakrishnan R, Mitchell D, Käs J, Ulvick S, Bilby C. Optical deformability as an inherent cell marker for testing malignant transformation and metastatic competence. Biophys J 2005;88:3689–3698.
Ha CH, Lee SC, Kim S, Chung J, Bae H, Kwon K. Novel mechanism of gene transfection by low-energy shock wave. Sci Rep 2015;5:12843.
Hall J. Unravelling the general properties of siRNAs: Strength in numbers and lessons from the past. Nat Rev Genet 2004;5:552–557.
Huber PE, Jenne J, Debus J, Wannenmacher MF, Pfisterer P. A comparison of shock wave and sinusoidal-focused ultrasound-induced localized transfection of HeLa cells. Ultrasound Med Biol 1999;25:1451–1457.
International Electrotechnical Commission (IEC). IEC61846 I. 61846 ultrasonics-pressure pulse lithotriptors—Characteristics of fields. Geneva: International Electrotechnical Commission; 1998.
Juffermans LJ, Meijering BD, Henning RH, Deelman LE. Ultrasound and microbubble-targeted delivery of small interfering RNA into primary endothelial cells is more effective than delivery of plasmid DNA. Ultrasound Med Biol 2014;40:532–540.
Karshafian R, Bevan PD, Williams R, Samac S, Burns PN. Sonoporation by ultrasound-activated microbubble contrast agents: Effect of acoustic exposure parameters on cell membrane permeability and cell viability. Ultrasound Med Biol 2009;35:847–860.
Khalil IA, Kogure K, Akita H, Harashima H. Uptake pathways and subsequent intracellular trafficking in nonviral gene delivery. Pharmacol Rev 2006;58:32–45.
Lauer U, Bürgelt E, Squire Z, Messmer K, Hofschneider P, Gregor M, Delius M. Shock wave permeabilization as a new gene transfer method. Gene Ther 1997;4:710–715.
Li X, Zhao X, Fang Y, Jiang X, Duong T, Fan C, Huang CC, Kain SR. Generation of destabilized green fluorescent protein as a transcription reporter. J Biol Chem 1998;273:34970–34975.
Madersbacher S, Marberger M. High-energy shockwaves and extracorporeal high-intensity focused ultrasound. J Endourol 2003;17:667–672.
Mehier-Humbert S, Guy RH. Physical methods for gene transfer: Improving the kinetics of gene delivery into cells. Adv Drug Deliv Rev 2005;57:733–753.
Millán-Chiu B, Camacho G, Varela-Echavarría A, Tamariz E, Fernández F, López-Marín LM, Loske AM. Shock waves and DNA-cationic lipid assemblies: A synergistic approach to express exogenous genes in human cells. Ultrasound Med Biol 2014;40:1599–1608.
Miller DL, Bao S, Gies RA, Thrall BD. Ultrasonic enhancement of gene transfection in murine melanoma tumors. Ultrasound in Med Biol 1999;25:1425–1430.
Mo S, Coussios CC, Seymour L, Carlisle R. Ultrasound-enhanced drug delivery for cancer. Expert Opin Drug Deliv 2012;9:1525–1538.
Murata R, Nakagawa K, Ohtori S, Ochiai N, Arai M, Saisu T, Sasho T, Takahashi K, Moriya H. The effects of radial shock waves on gene transfer in rabbit chondrocytes in vitro. Osteoarthritis Cartilage 2007;15:1275–1282.
Oosterhof G, Smits G, De Ruyter J, Van Moorselaar R, Schalken J, Debruyne F. The in vitro effect of electromagnetically generated shock waves (Lithostar) on the Dunning R3327 PAT-2 rat prostatic cancer cell-line. Urol Res 1989;17:13–19.
Pinel K, Lacoste J, Plane G, Ventura M, Couillaud F. Long-term in vivo imaging of translated RNAs for gene therapy. Gene Ther 2014;21:434–439.
Ponsaerts P, Van Tendeloo V, Berneman Z. Cancer immunotherapy using RNA-loaded dendritic cells. Clin Exp Immunol 2003;134:378–384.
Schwake G, Youssef S, Kuhr JT, Gude S, David MP, Mendoza E, Frey E, Rädler JO. Predictive modeling of non-viral gene transfer. Biotechnol Bioeng 2010;105:805–813.
Smith N, Sankin G, Simmons W, Nanke R, Fehre J, Zhong P. A comparison of light spot hydrophone and fiber optic probe hydrophone for lithotripter field characterization. Rev Sci Instrum 2012;83:014301.
Song J, Tata D, Li L, Taylor J, Bao S, Miller DL. Combined shock-wave and immunogene therapy of mouse melanoma and renal carcinoma tumors. Ultrasound Med Biol 2002;28:957–964.
Weihs AM, Fuchs C, Teuschl AH, Hartinger J, Slezak P, Mittermayr R, Redl H, Junger WG, Sitte HH, Rünzler D. Shock wave treatment enhances cell proliferation and improves wound healing by ATP release-coupled extracellular signal-regulated kinase (ERK) activation. J Biol Chem 2014;289:27090–27104.
Wells D. Gene therapy progress and prospects: electroporation and other physical methods. Gene Ther 2004;11:1363–1369.